SCIENCE CHINA
Chemistry

•REVIEWS•

October 2019 Vol.62 No.10: 1333–1345
https://doi.org/10.1007/s11426-019-9523-x

Application of electrochemistry to single-molecule junctions: from construction to modulation

Gan Wang[1], Biao-Feng Zeng[1], Shi-Qiang Zhao[2], Qiao-Zan Qian[2], Wenjing Hong[2] & Yang Yang[1*]

[1]*Pen-Tung Sah Institute of Micro-Nano Science and Technology, Xiamen University, Xiamen 361005, China;*
[2]*College of Chemistry and Chemical Engineering, Xiamen University, Xiamen 361005, China*

Received May 9, 2019; accepted June 27, 2019; published online August 13, 2019

State-of-the-art molecular electronics focus on the measurement of electrical properties of materials at the single-molecule level. Experimentally, molecular electronics face two primary challenges. One challenge is the reliable construction of single-molecule junctions, and the second challenge is the arbitrary modulation of electron transport through these junctions. Over the past decades, electrochemistry has been widely adopted to meet these challenges, leading to a wealth of novel findings. This review starts from the application of electrochemical methods to the fabrication of nanogaps, which is an essential platform for the construction of single-molecule junctions. The utilization of electrochemistry for the modification of molecular junctions, including terminal groups and structural backbones, is introduced, and finally, recent progress in the electrochemical modulation of single-molecule electron transport is reviewed.

single-molecule electronics, molecular junction, electrochemical deposition, electrochemical gating

Citation: Wang G, Zeng BF, Zhao SQ, Qian QZ, Hong W, Yang Y. Application of electrochemistry to single-molecule junctions: from construction to modulation. *Sci China Chem*, 2019, 62: 1333–1345, https://doi.org/10.1007/s11426-019-9523-x

1 Introduction

Molecular electronics represent the expansion of microelectronics to the molecular level, with the goal of using individual atoms, molecules, clusters, and supramolecules to construct functional devices [1–3]. In recent years, a number of molecular devices have been demonstrated as alternatives to silicon-based devices, including switches [4,5], rectifiers [6,7], sensors [8,9], and molecular transistors [10,11]. The concept of molecular electronics was first introduced in 1974, when Aviram *et al*. [12] found that a single molecule consisting of electron-accepting and electron-donating groups could behave as a rectifier. Subsequently, numerous researchers have pursued molecular electronics, leading to rapid growth in both theoretical approaches and experimental techniques. The latter can be achieved via two approaches. The first approach includes the development of new methods for building molecular junctions [13,14], such as scanning tunneling microscopy break junctions (STM-BJs) [15,16], mechanically controllable break junctions (MCBJs) [17–19], conducting probe atomic force microscopy [20,21], on-wire lithography [22,23], electromigration [24,25], and oxidative lithography [9,26]. The second approach is based on investigations of the response of molecular junctions under an environmental stimulus such as a magnetic field [27,28], electrical field [29,30], illumination [31,32], or temperature change [33,34].

Electrochemistry is a well-established discipline that has been developed over the past centuries and has shed light on molecular electronics over the past two decades. For the construction of molecular junctions, several methods have been developed on the basis of electrochemistry, including

*Corresponding author (email: yangyang@xmu.edu.cn)

electrochemical STM-BJs [35], electrochemical MCBJs [36], and electrochemical deposition junctions [37]. These methods have led to a number of exciting discoveries regarding charge transport in a single molecule.

In this review, we focus on the role of electrochemistry in the construction and modulation of single-molecule junctions. Because a nanogap is generally considered as the precursor for a molecular junction, we initially introduce two break junction methods that have been extensively utilized for fabricating this structure. We report on several approaches developed for the combination of break junctions and electrochemical methods. In the second section, we review recent progress achieved via electrochemistry in the modulation of single-molecule charge transport. We introduce three methods, including the modification of terminal groups, redox state shifting, and transport level shifting. Finally, prospects for future work are discussed.

2 Application of electrochemistry in the construction of molecular junctions

In molecular electronics, a single-molecule junction is an essential prototype; thus, the preparation of nanogaps was the first step toward single-molecule junctions. Since the early 1990s, various tools, including break junctions and electrochemical methods, have been developed for the fabrication of nanogaps. In this section, we describe these individual methods and then review the combination of break junctions and electrochemical methods.

2.1 Application of break junctions and electrochemistry in nanogap fabrication

Break junction techniques have been extensively employed in single-molecule electronics. Although it was predicted that individual molecules and atoms would have promising electrical properties during the time of R. Feynman, it was the development of nanogap fabrication that finally confirmed these expectations. If a nanogap between two electrodes can be scaled to the size of a molecule, it is then simple to construct an electrode-molecule-electrode junction, and the electrical properties of the target molecule can be measured (Figure 1(a)). For the construction of a nanogap, the major advantage of a break junction lies in the fine tuning of the nanometer-sized separation. This feature is crucial because even with the best instruments for electron beam lithography (EBL), it is difficult to fabricate a gap with a distribution on the scale of 1–10 nm [38,39]. The break junction method is based on the fact that at some time point during the dynamic opening and closing of a gap over thousands of cycles, the gap size will be comparable with the size of the target molecule. At this point, the target molecule

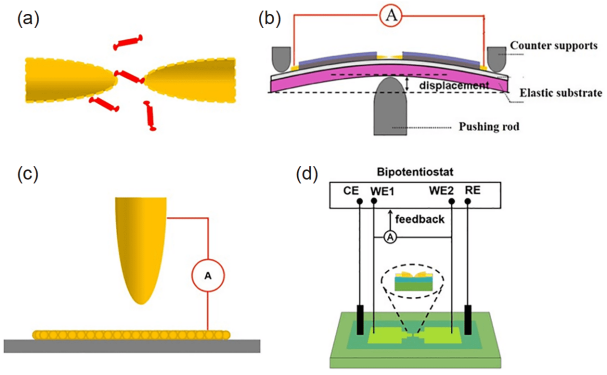

Figure 1 Schematic of (a) a target molecule assembled within a nanogap, (b) an MCBJ, (c) an STM-BJ, and (d) electrodeposition for the fabrication of a nanogap (color online).

can be captured and measured if the electrical apparatus have a sufficient sampling rate.

Among various break junction methods, STM-BJs and MCBJs are the most common. As early as the 1990s, Muller *et al*. [40] used MCBJs to fabricate and measure the electrical properties of metallic atomic point contacts. In 1997, Reed *et al*. [19] published the first report on the extension of MCBJs to the electrical measurement of single molecules. The architecture of an MCBJ consists of three components (Figure 1(b)): an elastic substrate with two configured electrodes, two stationary rods (counter support), and a pushing rod controlled by a stepper motor and/or a piezoelectric transducer. By controlling the movement of the pushing rod, an adjustable nanometer-sized gap can be created between the two electrodes to accommodate a single molecule.

For STM-BJs, the control modules consist of a piezoelectric transducer placed on the STM tip. In the operation of an STM-BJ, the tip is first driven toward the substrate until it contacts the substrate. Then, the tip is pulled out of contact with the substrate, and a nanogap is established (Figure 1(c)). In 2003, Xu *et al*. [15] introduced the use of statistics to break junction methods. These researchers employed an STM-BJ to perform conductance measurements of a single-molecule junction by repeatedly opening and closing the nanogap over thousands of cycles within a short duration, during which the molecules were wired between the STM tip and substrate numerous times. With this strategy, the authors collected a large number of conductance traces for the target molecule. These traces were utilized to construct statistical conductance histograms, enabling the authors to identify the most probable value for single-molecule conductance.

Despite the success of break junction methods in the fabrication of nanogaps and atomic point contacts, issues arose in the extension of this method to molecular junctions. For nanogaps fabricated by break junction techniques, the lifetimes are so short, i.e., several milliseconds, so the as-fabricated nanogaps are not suitable for long-time char-

acterization or device application. To construct nanogaps with a longer lifetime, electrochemistry provides an alternative strategy. Benefiting from high sensitivity, electrochemical methods can be applied to construct nanogaps. Because the nanogap is fabricated by a non-mechanical method differing from the break junction methods, it is more stable, enabling more studies on metallic contacts and molecular junctions at both the single-atom and single-molecule level (Figure 1(d)).

In 1998, Li *et al*. [37] reported the construction of atomic point contacts by combining a modified STM with electrodeposition (Figure 2(a)). The system was constructed using a non-mechanical technique, in which both the tip and the substrate were placed in a solution containing metallic cations. Briefly, the authors first controlled the STM tip to be 10–150 nm from the substrate, and the tip potential was maintained at the Nernst equilibrium potential of the cations. Second, a slightly more positive potential was applied to the substrate. This potential caused the metallic cations to be deposited on the substrate, resulting in a connection, as indicated by the sharp increase in the monitored current traces. As the potential was adjusted, the atoms dissolved into the solution, resulting in a narrow constriction for the study of conductance quantization.

To generate nanogaps with greater stability, a feedback system was applied to this combined method [41]. First, the authors used EBL to fabricate pairs of Au electrodes with a gap width of 20–60 nm. Then, cations were deposited on the gap between the two electrodes to reduce the width of the gap (Figure 2(b)). Because the gap width was less than 1 nm, the relationship between the tunneling current and the gap width followed $I_t \sim \exp(-ks)$, where s is the gap width, I_t is the tunneling current through the electrodes, and k is a constant with a value of 0.98±0.12 A^{-1}. This equation indicates that the tunneling current is sensitive to the gap size; therefore, the monitored tunneling current can be applied in a feedback system to fabricate a nanogap with atomic precision (Figure 2(c)). Furthermore, the processes of deposition and etching are switchable and reversible (Figure 2(d)). By adjusting the electrochemical potential, the researchers were able to control the alternation between deposition and etching to fabricate nanogaps with a high precision.

The chips constructed by these electrochemistry-based methods can easily be extended for the study of molecular junctions. Li *et al*. [42] added a 2,2′-bipyridine (22BPY) molecules to the chip and found that the conductance of the metal nanowire changed from 1 G_0 to 0.5 G_0 (Figure 3(a, b)). The authors then applied this method to study the electrical transport properties of individual polyaniline polymers [43] (Figure 3(c)). They demonstrated that by regulating the potential, the polyaniline could be continuously switched between two states, demonstrating its potential for application as a molecular switch (Figure 3(d)).

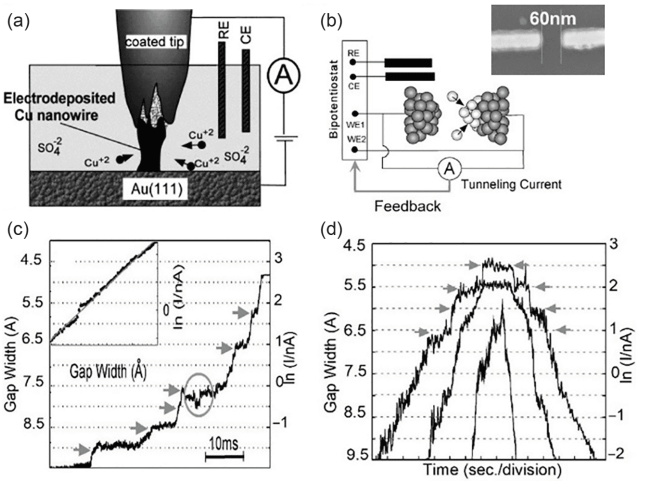

Figure 2 Fabrication schematic of a nanogap based on the combination of electrodeposition and (a) STM [37] and (b) EBL methods; (c) evolution of the tunneling current as a function of the gap width; (d) reversibility of the deposition and etching processes [41].

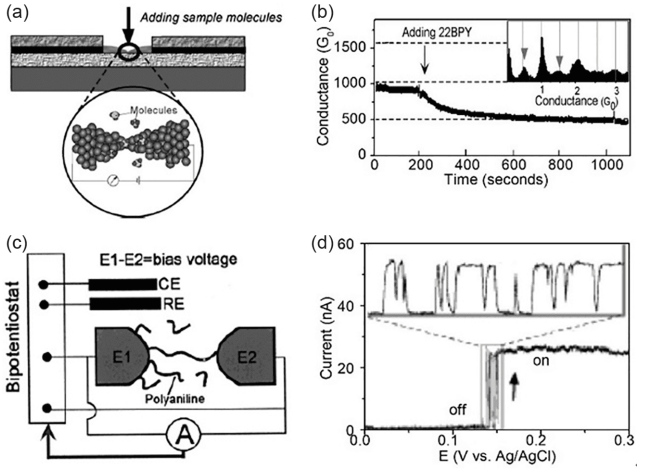

Figure 3 (a) Schematic of the construction of stable Cu nanowires for sensing molecules; (b) one thousand measurements of the conductance of Cu nanowires with the adsorption of 22BPY [42]; (c) schematic of the formation of a polyaniline nanojunction; (d) switching between a conducting state and an insulating state by potential regulation [43].

Compared with break junction methods, electrochemical methods can be applied fabricate highly stable nanogaps due to their non-dynamic principles and are more compatible with other characterization techniques such as Raman spectroscopy. Moreover, the as-fabricated nanogaps are more similar to practical devices than those produced by break junction techniques. However, two major challenges remain for electrochemical methods: the low success rate in the construction of molecular junctions and the uncertainty in the number of molecules that contribute to the measured electrical signals. These issues hinder the measurement of single-molecule transport by the use of electrochemical methods alone.

For practical applications in industry, micro-/nano-fabri-

cation techniques enable alternative strategies. These techniques have led to various promising devices such as molecular transistors [10,44] and molecular switches [5]. Recently, Gabriel *et al*. [45] combined nano-fabrication and self-assembled monolayer techniques to construct an array of molecular monolayer devices, which provides a route to the large-scale construction of molecular devices.

2.2 Application of electrochemical STM-BJs in the construction of molecular junctions

In 2005, Murakoshi *et al*. [46] developed a modified electrochemical STM technique, which combined conventional STM with electrodeposition. Figure 4(a) illustrates the working principle of this technique. Four electrodes are fabricated in an electrochemical cell, i.e., a reference electrode, a counter electrode, and two working electrodes (WE1 and WE2) composed of Au. With this electrode configuration, the deposition of metal cations (M) can be launched on both the tip and the substrate. Similar to the conventional STM-BJ technique, by moving the tip in and out of contact with the substrate, a nanoconstriction is created between the substrate and the tip. Using this technique, the researchers measured the electrical conductance of Ni atomic point contacts for different pH values and electrochemical potentials, as shown in Figure 4(b–d) [46]. They found that the electrochemical potential influences the conductance quantization and that hydrogen can help stabilize the Ni atomic point contact.

With this technique, the electrical conductances of various metals have been measured, including Cu [48], Pd [49], Rh [50], and Fe [51]. This technique has also been used to construct molecular junctions and measure their transport properties. As shown in Figure 4(e), Wang *et al*. [47] measured the conductance of succinic acid when it was wired between a Cu electrode pair and a Pd electrode pair. The authors found that the conductances of the Cu–(succinic acid)–Cu junction and Pd–(succinic acid)–Pd junction are 19 and 23 nS, respectively, which are consistent with measurements obtained by other techniques (Figure 4(f, g)).

However, it is difficult to extend this modified electrochemical STM technique to all types of metal materials. For both this technique and the traditional STM-BJ method, the tip and substrate are composed of the same metal materials. Both methods rely on the idea that an atomic point contact can be produced by crashing the tip into the substrate. However, this process depends on the ductility of the metal material, and some metals, such as Pd and Fe, do not exhibit atomic point contacts after such a crash. To overcome these problems, Zhou *et al*. [35] proposed a new approach termed the electrochemical jump-to-contact STM-BJ (ECSTM-BJ). Figure 5(a) illustrates the working principle of the ECSTM-BJ. The tip and substrate were prepared from the same metal

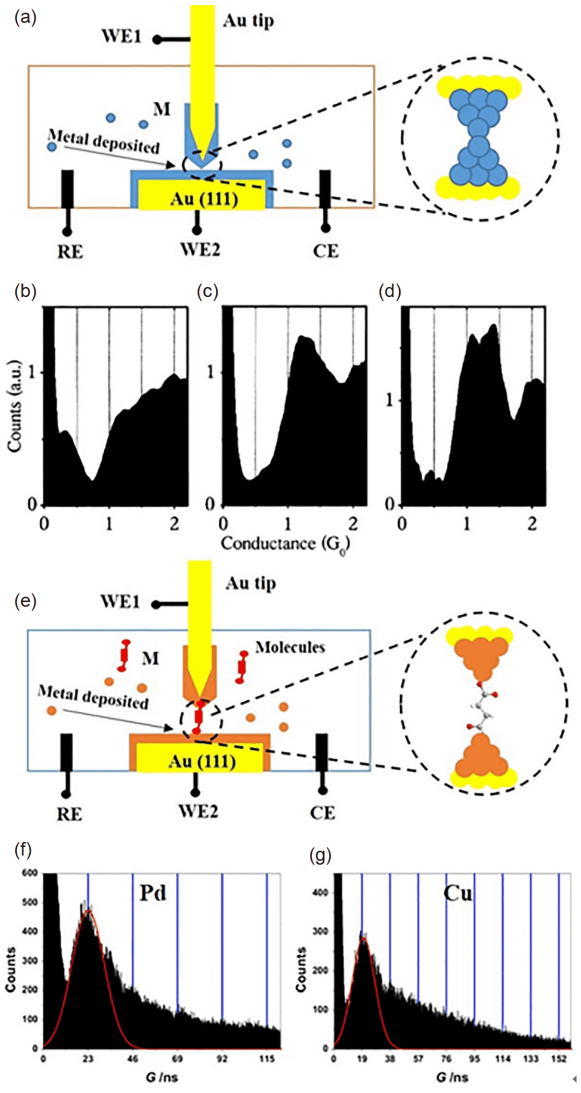

Figure 4 (a) Schematic of the modified electrochemical STM setup; conductance histograms of Ni nanoconstrictions for (b) −800 mV, pH 3.7, (c) −900 mV, pH 3.7, and (d) −800 mV, pH 2.3 [46]; (e) schematic of a modified electrochemical STM for the construction of single-molecule junctions; one-dimensional conductance histogram of (f) Cu–(succinic acid)–Cu and (g) Pd–(succinic acid)–Pd [47] (color online).

(M1), whereas the cation in solution is a different metal (M2). During typical operation of the ECSTM-BJ, the electrochemical potentials of the tip and substrate are modulated to ensure that deposition occurs only on the tip. A short voltage pulse is applied to the piezoelectric transducer in the control system, driving the tip toward the substrate. When the distance between the tip and substrate is sufficiently small, a jump-to-contact process occurs, in which some M2 atoms are transferred from the tip to the substrate, thus establishing a connection between the tip and substrate. At this point, the increased current through the tip and substrate triggers the feedback system. The tip is then moved upward to elongate the metal bridge, eventually resulting in atomic point contacts. By sequentially repeating the jump-to-

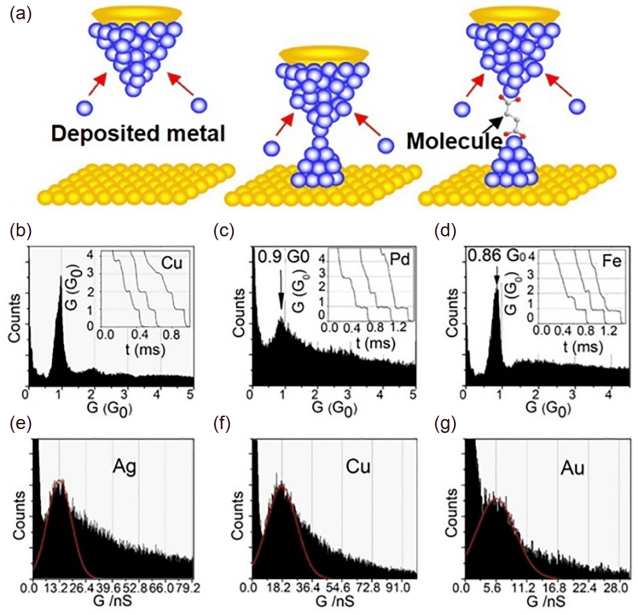

Figure 5 (a) Schematic of the use of ECSTM-BJ to construct an atomic point contact and a single-molecule junction [52]; conductance histograms of (b) Cu, (c) Pd, and (d) Fe (the insets present typical conductance traces) [35]; conductance histograms of single-molecule junctions of succinic acid wired between (e) Ag, (f) Cu and (g) Au electrode pairs [52] (color online).

contact and pulling processes thousands of times, a large number of conductance traces can be recorded to obtain statistical results (Figure 5(a)). By employing the ECSTM-BJ technique, the quantized conductance of various metals (Cu, Pd, and Fe) has been investigated, as shown in Figure 5 (b–d). It should be noted that for Pd and Fe, conductance measurements are difficult to perform using the traditional STM-BJ approach.

ECSTM-BJ has also been used to construct single-molecule junctions. Zhou *et al*. [52] investigated the charge transport through succinic acid with different metallic electrodes (Cu, Ag, and Au). For Ag and Cu metallic electrodes, the conductance values of the molecular junctions were 13.2 and 18.2 nS (Figure 5(e, f)), respectively, whereas a value of 5.6 nS was observed for Au electrodes (Figure 5(g)). This finding indicates that the interaction between the probe molecule and the metal follows the order of Cu>Au>Ag. In 2014, Wang *et al*. [47] used an ECSTM-BJ to measure the conductance of HOOC–$(CH_2)_n$–COOH (n=1–5) bound to different metals. The authors found that compared with Cu and Ag, Pd can enhance the charge transport through a molecular junction.

2.3 Application of electrochemical MCBJs in the construction of molecular junctions

Compared with STM-BJs, MCBJs exhibit greater mechanical stability and are easier to modify [17]. Numerous methods have been developed to fabricate MCBJ chips, such as EBL [53] and the notched-wire method. Chips fabricated by EBL can generate more stable and adjustable gaps, but this method is more expensive and time-consuming. The notched-wire method is convenient and rapid; however, the reduction ratio of the as-fabricated chip is usually two orders of magnitude smaller than that of a chip fabricated by EBL. Electrochemistry provides a new strategy to bridge the gap between the EBL and notched-wire methods. Li *et al*. [36] demonstrated a combined MCBJ and electrochemical deposition/etching method (electrochemical MCBJ) to study electrical transport through atomic point contacts and single molecules. The chip used in their experiments was fabricated in four steps. First, the researchers used photolithography to fabricate two Au electrodes separated by a ~1 μm gap on a Si substrate. Second, to reduce the ionic leakage current, a Si_3N_4 layer was deposited onto the Au electrodes as an insulation layer, leaving only a small amount of gold exposed. Third, the authors etched a groove into the Si beneath the gold electrodes to fabricate suspended electrodes. Finally, the gap between the electrodes was reduced by depositing Au onto the electrodes, and an atomic point contact was formed. The authors used the pushing rod of the MCBJ to adjust the gap of the chip and measured the electrical conductance of a Ni atomic point contact and a 4,4′-bipyridine molecular junction. This method is inexpensive and convenient for fabricating nanogaps. However, the etching of the Si substrate renders the system more fragile, which reduced the repeatability of sequential MCBJ operations.

To obtain a suspended electrode configuration without etching the Si substrate, Yang *et al*. [54] introduced a sacrificial layer to the electrochemical MCBJ system. The researchers fabricated a thin film on the Si substrate to serve as a sacrificial layer, such as a thermal oxidation SiO_2 layer or polyimide (PI) layer. The sacrificial layer was then removed by an etching technique. Specifically, wet-etching was applied for the thermal oxidation SiO_2 layer, and dry-etching was performed for the PI layer. With this modification, they found that the success rate of the subsequent MCBJ operation was improved. In 2010, Tian *et al*. [55] applied this improved electrochemical MCBJ method to fabricate and adjust a nanogap and to measure current-voltage (*I*-*V*) curves of an Au/BDT/Au junction, where BDT represents benzene-1,4-dithiol. In 2011, Yang *et al*. [56] further optimized the micro-fabrication process and demonstrated that by moving the notched structure from the Si substrate to the sacrificial layer above it, MCBJ operation could be performed over thousands of cycles. The authors termed this improved electrochemical MCBJ method as EC-MCBJ. The layer arrangement for the EC-MCBJ chip is shown in Figure 6(a), as well as the fabrication process, and the corresponding scanning electron microscope (SEM) characterization is given in Figure 6(b, c). Using this method, the authors investigated the influences of stretching speed, breakdown-

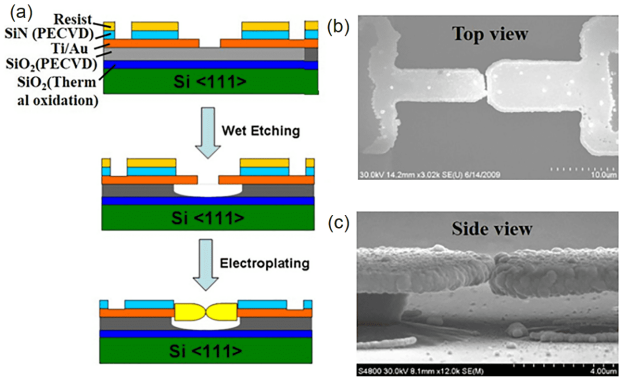

Figure 6 (a) Layer arrangement and fabrication process of the EC-MCBJ chip [55]; SEM images of the electrode pair in a typical EC-MCBJ chip from (b) top and (c) side views [56] (color online).

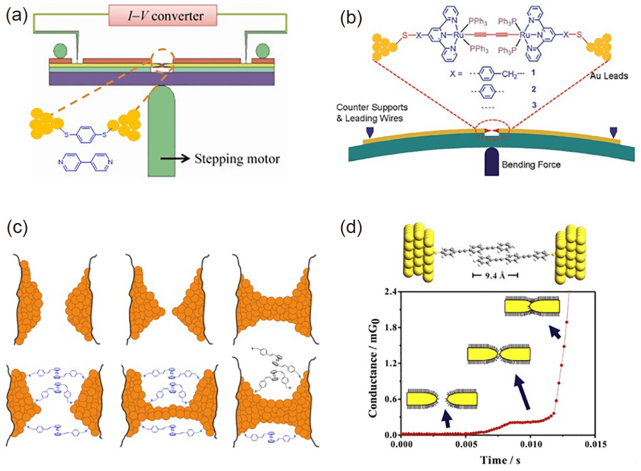

Figure 7 Application of an EC-MCBJ (a) to measure the single-molecule conductance of BDT and BPY [57] and (b) three 1,3-butadiyne-linked binuclear ruthenium(II) organometallic wires [58], (c) to study the microscopic evolution of a molecular junction as the electrodes approach each other in the presence of different molecules [59], and (d) to investigate charge transport through weak intramolecular interactions [61] (color online).

formation cycles, and degree of contact in the process of fabricating Au atomic point contacts. They found that reducing the stretching speed and degree of contact increases the probability for the formation of an atomic point contact.

To demonstrate the feasibility of the EC-MCBJ method in studying molecular junctions, as illustrated in Figure 7(a), Yang *et al*. [57] extended the EC-MCBJ to the construction of BDT and 4,4′-bipyridine (BPY) single-molecule junctions. The researchers measured the conductance for these two probe molecules by measuring the *I*-*V* curves and conductance histograms, and the results agreed with previously reported values obtained by traditional STM-BJ and MCBJ methods. To further verify the capability of this method for complex systems, Wen *et al*. [58] applied an EC-MCBJ to measure the conductance of three 1,3-butadiyne-linked binuclear ruthenium(II) organometallic wires, as shown in Figure 7(b). The authors found that these molecules exhibited a higher conductance than oligo(phenylene-ethynylene) compounds [5] of similar length and attributed this enhanced charge transport to the level alignment induced by the implantation of Ru atoms.

Furthermore, Yang *et al*. [59] adopted the EC-MCBJ method to study the microscopic evolution of a molecular junction as the two electrodes approached each other. The authors designed three molecules with varying rigidities to serve as probe molecules and monitored the evolution of their *I*-*V* curves as the nanogap was gradually closed. Unexpected *I*-*V* curves were observed in the presence of a ferrocene-bisvinylphenylmethyl dithiol and 1,3-butadiyne-linked dinuclear ruthenium(II) complex (Ru-1). On the basis of Kolb's jump-to-contact theory [60], the authors attributed the abnormal *I*-*V* curves to the response of the atomic contact under the stimulation of an electrical field (Figure 7(c)). EC-MCBJs have also been extended to the study of weak intramolecular interactions, such as π-π stacking. In 2016, Zheng *et al*. [61] measured *I*-*V* curves for a series of OPEs using the EC-MCBJ method. For the single-molecule conductance of OPEs, they observed that the values extracted from conductance histograms differed from those of measured *I*-*V* curves. From a detailed survey on the experimental protocols of histogram construction and *I*-*V* curve measurement, they demonstrated that different molecular configurations are established when using these two protocols. The difference arises because the protocol for *I*-*V* curve measurement relies on the closing process of the nanogap, whereas that of conductance histogram construction relies on the breaking process of the nanogap. As a result, in the *I*-*V* curve measurement, the π-π stacked OPE dimer contributes to the charge transport; meanwhile, in conductance histogram construction, the single-molecule OPE junction provides this contribution (Figure 7(d)).

These work unambiguously demonstrated that the EC-MCBJ method is reliable for constructing single-molecule junctions and for investigating charge transport at the single-molecule scale.

3 Transport modulation of molecular junctions by the electrochemical approach

Electrochemical methods are effective for constructing molecular junctions. In addition, these methods can also be applied to regulate the properties of electric transport at the single-molecule scale. On the basis of the working principle, the methods for electrochemical regulation of single-molecule transport can be divided into three classes: (1) modifying the terminal groups of molecules to enhance their coupling with the electrodes; (2) changing the molecular states between oxidation and reduction states; and (3) ad-

justing the transport level of the electrodes and/or the probe molecule. In this section, we describe the progress achieved in this field.

3.1 Transport modulation of molecular junctions by modifying molecule terminal groups

The metal-molecule interface plays a crucial role in the electrical transport properties of molecular devices [62–64]. Numerous studies have been reported on the relationship between charge transport and anchoring groups such as thiol [58,65], amino (–NH_2) [66], pyridine [67], and methyl-thiol (–SCH_3) [68]. In the large family of metal-molecule interactions in single-molecule electronics, the Au–C bond is distinct because a molecular junction is formed by a direct covalent bond. Compared with other interactions, the direct Au–C covalent bond gives rise to enhanced charge transport. In the early stages of single-molecule electronics, various precursors were identified for the construction of direct Au–C bonds, such as trimethyltin terminal groups [69,70] and trimethyl silyl groups [71,72]. These methods are efficient and reproducible; however, they do not allow *in situ* control of the formation and capture of molecular junctions.

Electrochemistry provides a new strategy to solve this problem. Electrochemistry can be applied to trigger dynamic chemical reactions in the anchoring groups, thus establishing more stable single-molecule junctions with *in situ* control. In 2013, Hines *et al*. [73] reported the first application of this electrochemical cleaving method to construct molecule junctions, as shown in Figure 8(a). The probe molecule in their work was a biphenyl compound with terminating groups of diazonium. With *in situ* control of the electrochemical potential, the terminal groups were broken off and the molecules bound to gold atoms. The cleavage process was confirmed by cyclic voltammetry. As shown in the inset of Figure 8(a), for the first cycle, an obvious reduction peak occurred near −650 mV, indicating that the diazonium groups were reduced. Moreover, no oxidation peak was found in the measured curve. The authors then used an STM-BJ to measure the conductance of the as-fabricated molecules under different electrochemical potentials. When the potential was controlled between 0 and −200 mV, no peaks were observed in the conductance histograms, implying that the reaction did not occur under these conditions. In contrast, when the potential was between −300 and −600 mV, a distinct peak appeared at ~2.3×10^{-3} G_0, indicating that the diazonium linker group had been reduced and cleaved off and that a stable Au–C bond had been established (Figure 8(b)).

Amine is one of the most widely used anchoring groups in the construction of molecular junctions. Recently, Zang *et al*. [74] measured the conductance of a series of oligophenylenediamines as varying biases were applied to the tip. The authors found that the conductance changed substantially

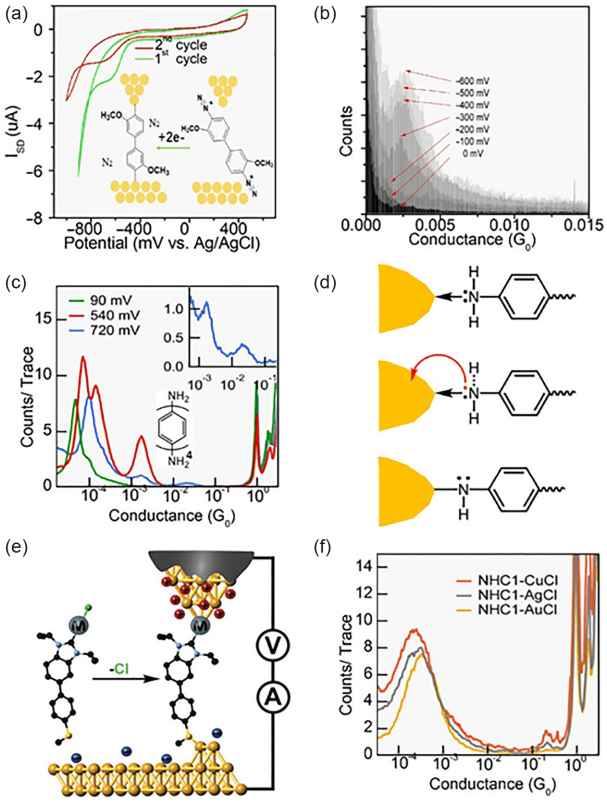

Figure 8 (a) Schematic of the electrochemical cleavage of the terminal groups of probe molecules. Inset: two successive cyclic voltammetry characterizations. (b) One-dimensional (1D) conductance histograms measured at different potentials [73]. (c) 1D conductance histograms of P4 at different potentials. (d) Formation of a new type of Au–N bond oxidation of a dative Au←N bond [74]. (e) Electrochemical reaction of a metal NHC complex to form a molecule-electrode contact. (f) 1D conductance histograms of NHC1-CuCl, NHC1-AgCl, and NHC1-AuCl [77] (color online).

compared with that obtained at a fixed bias. Only one peak (labeled as Low-G) was observed in the one-dimensional (1D) conductance histogram at a bias potential of 90 mV, which was attributed to a configuration in which the *p*-quaterphenylene-4,4‴-diamine (P4) molecule bound to gold atoms via two dative Au←N interactions. When a 540 mV bias was applied, another peak (labeled as High-G) emerged in the 1D conductance histogram in the high-conductance region. As the bias increased to 720 mV, an even higher conductance peak (Ultra-High-G) appeared (Figure 8(c)). These peaks indicate that the molecular junction was switchable in different conductance states. On the basis of theoretical calculations, the researchers attributed the High-G and Ultra-High-G peaks to the replacement of Au←N bonds by a new type of Au–N bond (Figure 8(d)). The *in situ* electrochemical reaction of the dative Au–N bond to a new type of Au–N bond can reduce the bond length and strengthen the coupling between the molecule and electrodes. The authors also constructed an *N*-heterocyclic carbene (NHC) molecular junction by modifying the anchoring group via an electrochemical approach [75]. Because of the in-

stability of the free carbenes, as well as their weak interaction with gold, it is difficult to measure the charge transport through the carbene molecular junction. In this work, the researchers adopted a novel strategy to form an NHC-electrode contact. First, a series of metal chloride complexes (MCl, M=Au, Ag, Cu) was coordinated at one end of benzannulated NHC (labeling the metal NHC complex as NHC1-MCl, M=Au, Ag, Cu). Then, the MCl was electrochemically reduced to M upon the application of a negative potential, resulting in NHC-electrode contacts (Figure 8(e)). With this experimental protocol, the authors measured the conductance of NHC1-MCl and found that for different metal materials, the charge transport followed the order of Au>Ag>Cu (Figure 8(f)).

3.2 Transport modulation of molecular junctions by changing the molecule redox state

Different structures have different influences on the electrical transport properties of molecular junctions. Electrochemistry can change the redox state of molecules, resulting in transport modulation of the electrical transport through the molecule.

In 2003, using a current-distance [$I(s)$; s=relative tip −sample distance] scanning method, Haiss *et al*. [76] studied the evolution of a single-molecule junction while altering its redox state via an electrochemical approach. The probe molecule used in this work was 6-[1′-(6-mercapto-hexyl)-[4,4′] bipyridinium]-hexane-1-thiol iodide (Figure 9(a)) [77], denoted as 6V6. A redox group is located in the middle of the backbone of 6V6, and the molecule is stable in both redox states. When the researchers applied a bias, they found that the conductance of 6V6 increased with decreasing bias in the region of 0.2 to −0.6 V (Figure 9(b)) [76]. They attributed the conductance increase to the reduction of the bipyridinium moiety (V) at negative potentials ($V^{2+}+e^{-}\rightarrow V^{+}$). In 2007, the authors further measured the conductance of 6V6 and obtained a complete curve for the conductance evolution of 6V6 as a function of potential (Figure 9(c, d)) [78]. Various redox-active molecular systems have been studied, such as ferrocene [79,80], transition metal complexes [81,82], tetrathiafulvalene [83,84], quinones [85], and proteins [86]. In these studies, the solvent, either an aqueous electrolyte or ionic liquid, provides an environment for the regulation of electrical transport through a single molecule. As a solvent, ionic liquids can provide a wider potential window than distilled water [77]. In 2012, Kay *et al*. [87] used STM-BJs to measure the conductance of pyrrolo-tetrathiafulvalene (pTTF) in an ionic liquid of 1-butyl-3-methylimidazolium trifluoromethanesulfonate (BMIOTf). It was demonstrated that only one redox state of pTTF could be investigated in aqueous electrolytes, whereas in ionic liquid electrolytes, three redox states of pTTF could be studied (Figure 9(e)). As

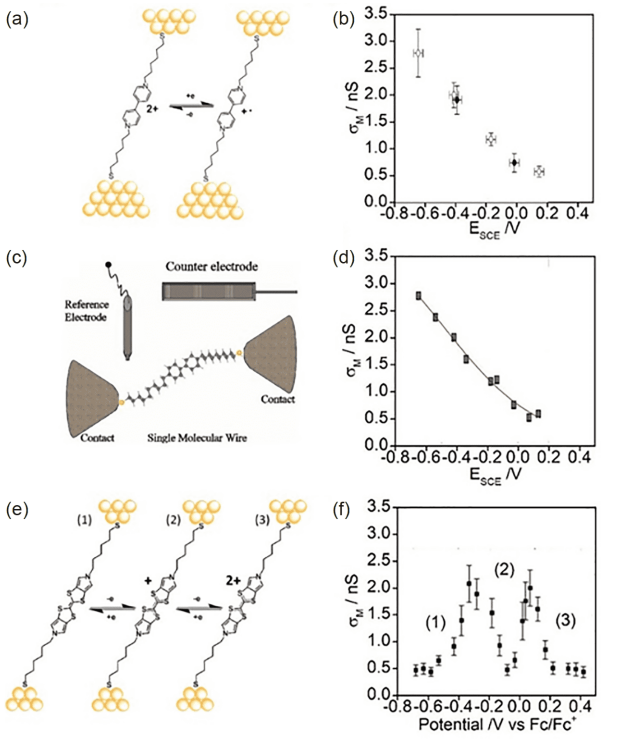

Figure 9 (a) Schematic of the electrochemical reaction of 6V6 [77]; (b) conductance of 6V6 at different potentials in aqueous solution [76]; (c) schematic of the electrochemical reaction of a single molecule in the electrochemical setup; (d) measurement of the conductance of 6V6 at different potentials (the red line provides a guide for the eye) [78]; (e) schematic of the electrochemical reaction of pTTF in ionic liquid; (f) conductance of pTTF at different potentials in ionic liquid [77] (color online).

the electrochemical potential was swept from −0.6 to 0.5 V, the single-molecule conductance was observed, exhibiting two peaks at −0.6–−0.15 V and −0.15–0.5 V (Figure 9(f)) [77]. The authors attributed the peaks to the switching of pTTF between different redox states.

Anthraquinone (Aq) [88] is a redox group that has been widely utilized for investigating reaction states at the single-molecule scale [89,90]. A distinct feature of Aq is that it can be reversibly oxidized and reduced. Xiang *et al*. [91] extended the STM-BJ to investigate the thermodynamics and redox kinetics of Aq at the single-molecule scale (Figure 10 (a, b)). The authors added Aq to a DNA strand and used single-molecule conductance measurements to detect the redox state of Aq. The conductance values of the oxidation state (Ox-Aq) and reduction state (Re-H_2Aq) were measured. In the constructed 1D conductance histograms, the peak area represents the number of Aq-DNA strands in each state. The researchers used a Gaussian function to fit the area of both the high-conductance and low-conductance peaks, which were attributed to Ox-Aq and Re-H_2Aq, respectively. The heights of the high- and low-conductance peaks exhibited equal increases and decreases as the potential was reduced, indicating that the molecule gradually evolved from the re-

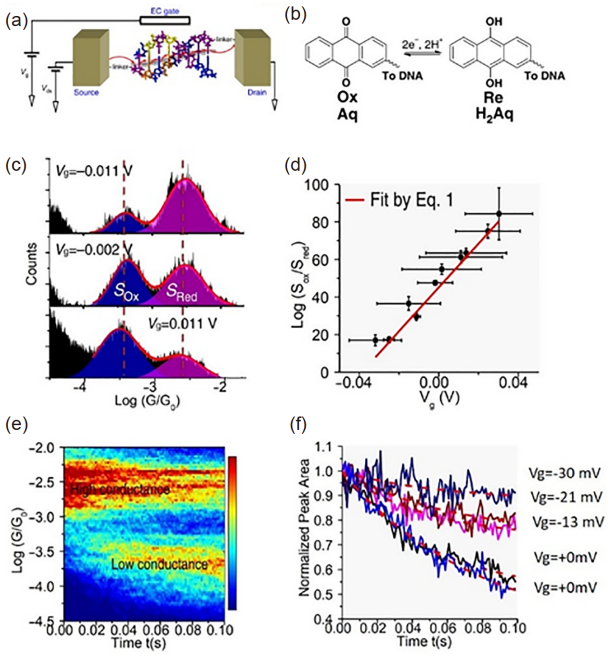

Figure 10 (a) Illustration of the electrochemically modulated STM-BJ technique. (b) Schematic of the reversible redox reaction of Aq-DNA. (c) One-dimensional conductance histograms at different potentials, where Gaussian fitting was employed to calculate the peak areas for oxidized and reduced Aq-DNA molecules. (d) Plot of log(S_{ox}/S_{red}) (S_{ox} and S_{red} are the areas of the low- and high-conductance peaks, respectively) at different potentials. Curve fitting was performed by using the Nernst equation (red solid line). (e) Two-dimensional conductance-time histogram at a potential of 0.000±0.005 V. (f) Normalized peak area of the high-conductance peak versus time for different potentials. The red dashed lines present curves fitted with a rate equation [91] (color online).

duction state to the oxidation state (Figure 10(c)). Furthermore, the authors found that the thermodynamic equilibrium of molecules in the oxidation and reduction states followed the Nernst equation (Figure 10(d)). To study the kinetics of the reaction, they applied a potential of 0.000±0.005 V to launch the reaction and measured the change in the relative amount of Aq molecules over time. From the slope of the curves, the forward rate (k_f) and backward rate constants of the reversible reaction were calculated (Figure 10(e, f)). Using this experimental protocol, in 2019, Li *et al.* [92] investigated the electrochemical reaction kinetics of a series of ferrocene derivatives composed of a ferrocene redox center and two varying alkane-thiol linkers. By performing numerical simulations of the data, the authors found that the reaction exhibited first-order kinetic behavior at the single-molecule scale.

3.3 Transport modulation of molecular junctions by shifting the energy levels of the electrode and molecule

Electrochemistry can change the electrical transport of a single molecule by changing the oxidation and reduction states. In addition, electrochemistry can also be applied to change the electrical transport of a single molecule by changing the energy-level alignment between the molecule and electrode. For an electrode-molecule-electrode junction, the Fermi level of the electrodes lies between the highest occupied molecular orbital (HOMO) and the lowest unoccupied molecular orbital (LUMO). The mismatch between the molecular transport level and the Fermi level of the electrode acts as a barrier that hinders single-molecule charge transport. By applying a potential, the energy levels of the electrode and/or molecule can be changed, thus modulating the barrier to single-molecule charge transport.

For molecules with a large HOMO-LUMO gap, such as alkane, both the HOMO and LUMO of the molecule are far from the Fermi level of the electrode. As a result, the applied potential does not significantly affect the conductance of the molecules. For molecules with a small HOMO-LUMO gap, the HOMO and LUMO are close to the Fermi level of the electrode [93]. In this case, the molecular conductance will change significantly with the potential.

Various methods have been developed to achieve electrochemical gating. On the basis of the electrode configuration, these methods can be divided into three classes: two-electrode, three-electrode, and four-electrode systems. Capozzi *et al.* [6] developed a two-electrode method based on the STM-BJ, where a wax-coated STM tip and the substrate act as two working electrodes (Figure 11(a)). Using this method, the authors found that the single-molecule junction behaved as a rectifier in a polar solvent. They applied a 180 mV bias between the tip and substrate, altered the bias polarity, and measured the conductance of four thiophene-1,1-dioxide (TDO4) in polar and nonpolar solvents. In polar solvents, the molecular conductance remained constant before and after the polarity was altered (Figure 11(c)). However, the conductance measured at a negative potential increased by as much as 3.25-fold over the value measured for a positive potential in polar solvents (Figure 11(d)). The authors also performed *I-V* curve measurements of three molecules with similar structures (three thiophene-1,1-dioxide (TDO3), TDO4, and five thiophene-1,1-dioxide (TDO5)), as shown in Figure 11(e, f). In nonpolar solvents, the *I-V* curves were symmetric, whereas in polar solvents, the molecules displayed a higher current at negative potentials than at positive potentials, indicating that these molecules exert a rectifying effect in polar solvents. For TDO3, TDO4, and TDO5, the rectification ratios were −4 at 0.6 V, −90 at 0.42 V, and −200 at 0.3 V, respectively. The researchers attributed the different results in polar and nonpolar solvents to an asymmetric electric double layer caused by the capsulated tip and substrate. Because the exposed area of the capsulated tip was much smaller than that of the substrate, a denser double layer was formed compared with that of the substrate. As a result, the level shifting varied as the bias polarity was altered, leading to rectifying behavior.

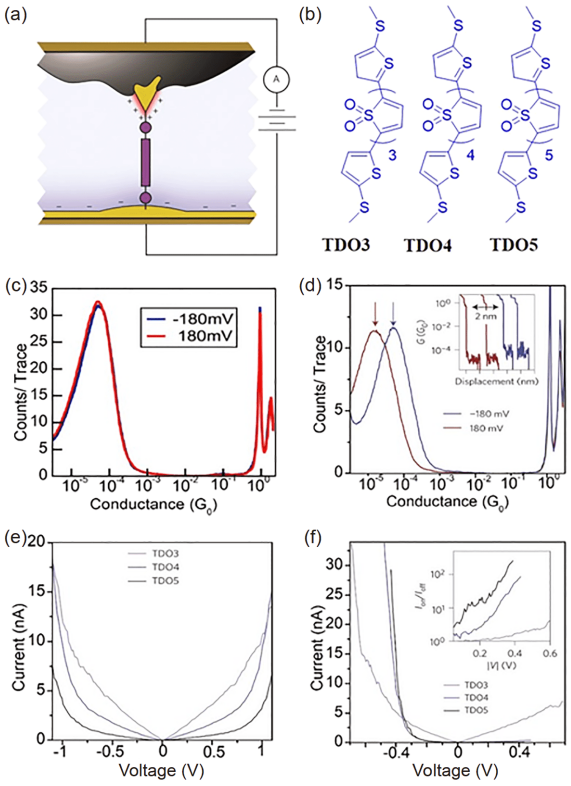

Figure 11 (a) Schematic of the modulation of single-molecule charge transport using the two-electrode method in a polar solvent. (b) Molecular structures of TDO3, TDO4, and TDO5. One-dimensional conductance histograms of TDO4 measured at −180 and 180 mV in (c) nonpolar solvent and (d) polar solvent. Insets: typical conductance curves. Averaged *I-V* curves for the three probe molecules in (e) nonpolar solvent and (f) polar solvent [6] (color online).

In 2014, Capozzi *et al*. [94] developed a three-electrode configuration for electrochemical gating. In addition to the wax-coated Au tip and Au substrate as two working electrodes, Pt was added as a counter electrode. The introduction of this third electrode enabled regulation of the double layer of the working electrodes. When a potential of a different polarity was applied to the counter electrode, the working electrodes responded to form a double layer with a different polarity, thus regulating the molecular orbital.

The two-electrode and three-electrode methods both rely on an electrochemical double layer. However, there is no independent reference electrode in these two methods. From the perspective of traditional electrochemistry, the electrochemical modulation would be inefficient under these conditions. An alternative strategy is to employ a four-electrode configuration. In particular, the capsulated Au tip and Au substrate of the STM serve as two working electrodes, and two additional electrodes are introduced into the system to act as a reference electrode and counter electrode. With this electrode configuration, the potentials of the tip and the substrate can be changed by maintaining a bias between them. The four-electrode method enables more accurate control of the electrode potential and is more efficient than the two-electrode and three-electrode methods in the gating of charge transport. More recently, significant progress on the modulation of single-molecule transport was achieved because of the extension of the four-electrode method to molecules exhibiting quantum interference (QI) effects [95–97]. Huang *et al*. [97] investigated the charge transport through *meta*- and *para*-benzene-based molecules with dihydrobenzo[*b*] thiophene as the anchoring group (*meta*-BT and *para*-BT) (Figure 12(a)). The transmission spectra for *meta*-BT and *para*-BT were calculated, as shown in Figure 12(b). The *meta*-BT and *para*-BT exhibit sharp-valleyed and flat-valleyed conductance as a function of the electrode potential. The authors measured the conductance of *meta*-BT and *para*-BT in an organic solvent (CH_2Cl_2) and ionic liquid (methylimidazolium hexafluorophosphate) ($BMIPF_6$). When a 50 mV bias was applied to the CH_2Cl_2 solution, the conductance of *para*-BT was $10^{-4.1}$ G_0, whereas the conductance of *meta*-BT was less than 10^{-6} G_0 and could not be detected (Figure 12(c)). When the researchers measured the conductance of *meta*-BT in ionic liquid, no conductance was detected at a bias of −0.4 V, similar to the result in organic solvent at a bias of 50 mV (Figure 12(d)). However, a peak

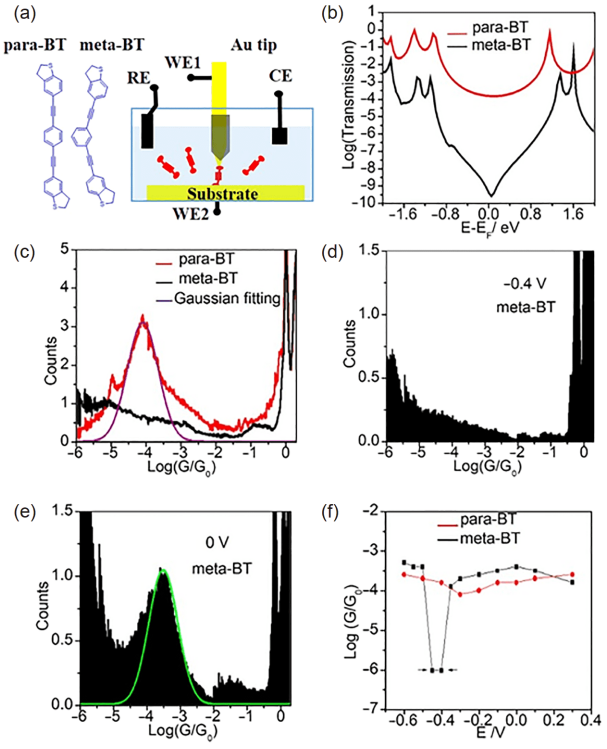

Figure 12 (a) Molecular structures of *para*-BT and *meta*-BT and schematic of the four-electrode method; (b) calculated transmission spectra for *para*-BT (red) and *meta*-BT (black); (c) one-dimensional (1D) conductance histograms of *para*-BT (red) and *meta*-BT (black) (the purple line presents Gaussian fitting results for the peak); (d) 1D conductance histogram of *meta*-BT measured at a potential of −0.4 V; (e) 1D conductance histogram of *para*-BT measured at a potential of 0 V; (f) conductance of *para*-BT (red) and *meta*-BT (black) as a function of potential [97] (color online).

arose upon the application of a bias to fix the potentials of the working electrodes at 0 V (Figure 12(e)). The different results observed at potentials of −0.4 and 0 V demonstrated that the charge transport properties of *meta*-BT varied as the potential was changed. Furthermore, the authors measured the conductance evolution of *para*-BT and *meta*-BT upon potential sweeping. The variation trends of *meta*-BT and *para*-BT were consistent with the transmission spectra. In particular, the variance of the conductance of *meta*-BT reached more than two orders of magnitude, and the maximum conductance was even greater than that of *para*-BT (Figure 12(f)). The difference between *para*-BT and *meta*-BT is attributed to the QI effect of the latter. These works indicated that electrochemistry can be applied to regulate the QI effect of molecules, providing a promising approach for the design of an effective molecular switch.

4 Conclusions and perspective

Break junction techniques can be applied to construct single-molecule junctions in a convenient manner, providing a platform for researchers to understand the electrical transport of individual atoms and molecules. The introduction of electrochemical methods broadens the scope of molecular electronics, aiding in the discovery of a number of novel physical and chemical phenomena. For the construction of molecular junctions, electrodeposition can be applied to fabricate an electrode pair with a precise and stable nanogap. By employing these nanogaps, various single-molecule junctions have been successfully constructed, and their electrical properties have been characterized. By changing the electroplating solution, the electrochemical deposition method can, in principle, be extended to a vast number of metals and other materials. Because different metals have different properties, particularly under external influences such as magnetic, thermal, and optical modulations, we foresee that further study of this subject will lead to numerous findings and will provide an in-depth understanding of the physical and chemical properties of molecular junctions. To regulate the electrical transport of a single molecule, many challenges remain. It is difficult to monitor and control the adsorption process of molecules on an electrode surface. Moreover, the microscopic configurations contributing to the measured electrical properties are usually assumed from theoretical simulations rather than experimental observations. Fortunately, these electrochemical approaches are compatible with most surface diagnostic techniques such as Raman spectroscopy [98,99], X-ray photoelectron spectroscopy, infrared spectroscopy, and SEM. The combination of electrical measurements and these methods can help to establish the correlation between structure and conducting activity. In summary, electrochemistry has aided and will continue to promote the development of molecular electronics.

Acknowledgements This work was supported by the Fundamental Research Funds for the Central Universities in China (Xiamen University: 20720170035), the National Natural Science Foundation of China (21503179, 61573295, 21722305), and the Nation Key R&D Program of China (2017YFA0204902). The authors thank Dr. Shu Hu and Dr. Chao Zhan for fruitful discussions.

Conflict of interest The authors declare that they have no conflict of interest.

1 Ratner M. *Nat Nanotech*, 2013, 8: 378–381
2 Lörtscher E. *Nat Nanotech*, 2013, 8: 381–384
3 Elke S, Carlos CJ. *Molecular Electronics: An Introduction to Theory and Experiment*. Vol. 15. Singapore: World Scientific, 2017
4 Su TA, Li H, Steigerwald ML, Venkataraman L, Nuckolls C. *Nat Chem*, 2015, 7: 215–220
5 Jia C, Migliore A, Xin N, Huang S, Wang J, Yang Q, Wang S, Chen H, Wang D, Feng B, Liu Z, Zhang G, Qu DH, Tian H, Ratner MA, Xu HQ, Nitzan A, Guo X. *Science*, 2016, 352: 1443–1445
6 Capozzi B, Xia J, Adak O, Dell EJ, Liu ZF, Taylor JC, Neaton JB, Campos LM, Venkataraman L. *Nat Nanotech*, 2015, 10: 522–527
7 Guo C, Wang K, Zerah-Harush E, Hamill J, Wang B, Dubi Y, Xu B. *Nat Chem*, 2016, 8: 484–490
8 Li Z, Smeu M, Afsari S, Xing Y, Ratner MA, Borguet E. *Angew Chem Int Ed*, 2014, 53: 1098–1102
9 Cao Y, Dong S, Liu S, He L, Gan L, Yu X, Steigerwald ML, Wu X, Liu Z, Guo X. *Angew Chem Int Ed*, 2012, 51: 12228–12232
10 Song H, Kim Y, Jang YH, Jeong H, Reed MA, Lee T. *Nature*, 2009, 462: 1039–1043
11 Perrin ML, Verzijl CJO, Martin CA, Shaikh AJ, Eelkema R, van Esch JH, van Ruitenbeek JM, Thijssen JM, van der Zant HSJ, Dulić D. *Nat Nanotech*, 2013, 8: 282–287
12 Aviram A, Ratner MA. *Chem Phys Lett*, 1974, 29: 277–283
13 Xiang D, Wang X, Jia C, Lee T, Guo X. *Chem Rev*, 2016, 116: 4318–4440
14 Huang C, Rudnev AV, Hong W, Wandlowski T. *Chem Soc Rev*, 2015, 44: 889–901
15 Xu B, Tao NJ. *Science*, 2003, 301: 1221–1223
16 Venkataraman L, Klare JE, Nuckolls C, Hybertsen MS, Steigerwald ML. *Nature*, 2006, 442: 904–907
17 Xiang D, Jeong H, Lee T, Mayer D. *Adv Mater*, 2013, 25: 4845–4867
18 Smit RHM, Noat Y, Untiedt C, Lang ND, van Hemert MC, van Ruitenbeek JM. *Nature*, 2002, 419: 906–909
19 Reed MA, Zhou C, Muller CJ, Burgin TP, Tour JM. *Science*, 1997, 278: 252–254
20 Cui XD, Primak A, Zarate X, Tomfohr J, Sankey OF, Moore AL, Moore TA, Gust D, Harris G, Lindsay SM. *Science*, 2001, 294: 571–574
21 Ho Choi S, Kim B, Frisbie CD. *Science*, 2008, 320: 1482–1486
22 Qin L, Park S, Huang L, Mirkin CA. *Science*, 2005, 309: 113–115
23 Banholzer MJ, Qin L, Millstone JE, Osberg KD, Mirkin CA. *Nat Protoc*, 2009, 4: 838–848
24 Park J, Pasupathy AN, Goldsmith JI, Chang C, Yaish Y, Petta JR, Rinkoski M, Sethna JP, Abruña HD, McEuen PL, Ralph DC. *Nature*, 2002, 417: 722–725
25 Liang W, Shores MP, Bockrath M, Long JR, Park H. *Nature*, 2002, 417: 725–729
26 Guo X, Small JP, Klare JE, Wang Y, Purewal MS, Tam IW, Hong BH, Caldwell R, Huang L, O'brien S, Yan J, Breslow R, Wind SJ, Hone J, Kim P, Nuckolls C. *Science*, 2006, 311: 356–359
27 Thiele S, Balestro F, Ballou R, Klyatskaya S, Ruben M, Wernsdorfer

W. *Science*, 2014, 344: 1135–1138
28 Natterer FD, Yang K, Paul W, Willke P, Choi T, Greber T, Heinrich AJ, Lutz CP. *Nature*, 2017, 543: 226–228
29 Aragonès AC, Haworth NL, Darwish N, Ciampi S, Bloomfield NJ, Wallace GG, Diez-Perez I, Coote ML. *Nature*, 2016, 531: 88–91
30 Ciampi S, Darwish N, Aitken HM, Díez-Pérez I, Coote ML. *Chem Soc Rev*, 2018, 47: 5146–5164
31 Huang C, Jevric M, Borges A, Olsen ST, Hamill JM, Zheng JT, Yang Y, Rudnev A, Baghernejad M, Broekmann P, Petersen AU, Wandlowski T, Mikkelsen KV, Solomon GC, Brøndsted Nielsen M, Hong W. *Nat Commun*, 2017, 8: 15436
32 Chen L, Feng A, Wang M, Liu J, Hong W, Guo X, Xiang D. *Sci China Chem*, 2018, 61: 1368–1384
33 Reddy P, Jang SY, Segalman RA, Majumdar A. *Science*, 2007, 315: 1568–1571
34 Cui L, Miao R, Wang K, Thompson D, Zotti LA, Cuevas JC, Meyhofer E, Reddy P. *Nat Nanotech*, 2018, 13: 122–127
35 Zhou XS, Wei YM, Liu L, Chen ZB, Tang J, Mao BW. *J Am Chem Soc*, 2008, 130: 13228–13230
36 Li XL, Hua SZ, Chopra HD, Tao NJ. *Micro Nano Lett*, 2006, 1: 83–88
37 Li CZ, Tao NJ. *Appl Phys Lett*, 1998, 72: 894–896
38 Nedelcu M, Saifullah MSM, Hasko DG, Jang A, Anderson D, Huck WTS, Jones GAC, Welland ME, Kang DJ, Steiner U. *Adv Funct Mater*, 2010, 20: 2317–2323
39 Haedler AT, Kreger K, Issac A, Wittmann B, Kivala M, Hammer N, Köhler J, Schmidt HW, Hildner R. *Nature*, 2015, 523: 196–199
40 Muller C, van Ruitenbeek JM J, de Jongh LJ L. *Phys Rev Lett*, 1992, 69: 140–143
41 Li CZ, He HX, Tao NJ. *Appl Phys Lett*, 2000, 77: 3995–3997
42 Li CZ, He HX, Bogozi A, Bunch JS, Tao NJ. *Appl Phys Lett*, 2000, 76: 1333–1335
43 He H, Zhu J, Tao NJ, Nagahara LA, Amlani I, Tsui R. *J Am Chem Soc*, 2001, 123: 7730–7731
44 Xiang D, Jeong H, Kim D, Lee T, Cheng Y, Wang Q, Mayer D. *Nano Lett*, 2013, 13: 2809–2813
45 Puebla-Hellmann G, Venkatesan K, Mayor M, Lörtscher E. *Nature*, 2018, 559: 232–235
46 Kiguchi M, Konishi T, Murakoshi K. *Appl Phys Lett*, 2005, 87: 043104
47 Wang YH, Zhou XY, Sun YY, Han D, Zheng JF, Niu ZJ, Zhou XS. *Electrochim Acta*, 2014, 123: 205–210
48 Kiguchi M, Konishi T, Miura S, Murakoshi K. *Nanotechnology*, 2007, 18: 424011
49 Kiguchi M, Murakoshi K. *Appl Phys Lett*, 2006, 88: 253112
50 Konishi T, Kiguchi M, Murakoshi K. *Phys Rev B*, 2010, 81: 125422
51 Konishi T, Kiguchi M, Murakoshi K. *Surf Sci*, 2008, 602: 2333–2336
52 Zhou XS, Liang JH, Chen ZB, Mao BW. *Electrochem Commun*, 2011, 13: 407–410
53 Lörtscher E, Ciszek JW, Tour J, Riel H. *Small*, 2006, 2: 973–977
54 Yang Y, Tian JH, Luo ZZ, Wu ST, Tian ZQ. *J Mater Eng*, 2008, 36: 278–286
55 Tian JH, Yang Y, Liu B, Schöllhorn B, Wu DY, Maisonhaute E, Muns AS, Chen Y, Amatore C, Tao NJ, Tian ZQ. *Nanotechnology*, 2010, 21: 274012
56 Yang Y, Liu JY, Chen ZB, Tian JH, Jin X, Liu B, Li X, Luo ZZ, Lu M, Yang FZ, Tao N, Tian ZQ. *Nanotechnology*, 2011, 22: 275313
57 Yang Y, Chen Z, Liu J, Lu M, Yang D, Yang F, Tian Z. *Nano Res*, 2011, 4: 1199–1207
58 Wen HM, Yang Y, Zhou XS, Liu JY, Zhang DB, Chen ZB, Wang JY, Chen ZN, Tian ZQ. *Chem Sci*, 2013, 4: 2471–2477
59 Yang Y, Liu J, Feng S, Wen H, Tian J, Zheng J, Schöllhorn B, Amatore C, Chen Z, Tian Z. *Nano Res*, 2016, 9: 560–570
60 Kolb D, Ullmann R, Will T. *Science*, 1997, 275: 1097–1099
61 Zheng JT, Yan RW, Tian JH, Liu JY, Pei LQ, Wu DY, Dai K, Yang Y, Jin S, Hong W, Tian ZQ. *Electrochim Acta*, 2016, 200: 268–275
62 Chen F, Li X, Hihath J, Huang Z, Tao N. *J Am Chem Soc*, 2006, 128: 15874–15881
63 Hong W, Manrique DZ, Moreno-García P, Gulcur M, Mishchenko A, Lambert CJ, Bryce MR, Wandlowski T. *J Am Chem Soc*, 2012, 134: 2292–2304
64 Leary E, La Rosa A, González MT, Rubio-Bollinger G, Agraït N, Martín N. *Chem Soc Rev*, 2015, 44: 920–942
65 Huang Z, Chen F, Bennett PA, Tao N. *J Am Chem Soc*, 2007, 129: 13225–13231
66 Venkataraman L, Klare JE, Tam IW, Nuckolls C, Hybertsen MS, Steigerwald ML. *Nano Lett*, 2006, 6: 458–462
67 Xu B, Xiao X, Tao NJ. *J Am Chem Soc*, 2003, 125: 16164–16165
68 Zhang YP, Chen LC, Zhang ZQ, Cao JJ, Tang C, Liu J, Duan LL, Huo Y, Shao X, Hong W, Zhang HL. *J Am Chem Soc*, 2018, 140: 6531–6535
69 Cheng ZL, Skouta R, Vazquez H, Widawsky JR, Schneebeli S, Chen W, Hybertsen MS, Breslow R, Venkataraman L. *Nat Nanotech*, 2011, 6: 353–357
70 Chen W, Widawsky JR, Vázquez H, Schneebeli ST, Hybertsen MS, Breslow R, Venkataraman L. *J Am Chem Soc*, 2011, 133: 17160–17163
71 Hong W, Li H, Liu SX, Fu Y, Li J, Kaliginedi V, Decurtins S, Wandlowski T. *J Am Chem Soc*, 2012, 134: 19425–19431
72 Huang C, Chen S, Baruël Ørnsø K, Reber D, Baghernejad M, Fu Y, Wandlowski T, Decurtins S, Hong W, Thygesen KS, Liu SX. *Angew Chem Int Ed*, 2015, 54: 14304–14307
73 Hines T, Díez-Pérez I, Nakamura H, Shimazaki T, Asai Y, Tao N. *J Am Chem Soc*, 2013, 135: 3319–3322
74 Zang Y, Pinkard A, Liu ZF, Neaton JB, Steigerwald ML, Roy X, Venkataraman L. *J Am Chem Soc*, 2017, 139: 14845–14848
75 Doud EA, Inkpen MS, Lovat G, Montes E, Paley DW, Steigerwald ML, Vázquez H, Venkataraman L, Roy X. *J Am Chem Soc*, 2018, 140: 8944–8949
76 Haiss W, van Zalinge H, Higgins SJ, Bethell D, Höbenreich H, Schiffrin DJ, Nichols RJ. *J Am Chem Soc*, 2003, 125: 15294–15295
77 Nichols RJ, Higgins SJ. *Acc Chem Res*, 2016, 49: 2640–2648
78 Haiss W, Albrecht T, van Zalinge H, Higgins SJ, Bethell D, Höbenreich H, Schiffrin DJ, Nichols RJ, Kuznetsov AM, Zhang J, Chi Q, Ulstrup J. *J Phys Chem B*, 2007, 111: 6703–6712
79 Xiao X, Brune D, He J, Lindsay S, Gorman CB, Tao N. *Chem Phys*, 2006, 326: 138–143
80 Zhou XS, Liu L, Fortgang P, Lefevre AS, Serra-Muns A, Raouafi N, Amatore C, Mao BW, Maisonhaute E, Schollhorn B. *J Am Chem Soc*, 2011, 133: 7509–7516
81 Albrecht T, Guckian A, Kuznetsov AM, Vos JG, Ulstrup J. *J Am Chem Soc*, 2006, 128: 17132–17138
82 Ricci AM, Calvo EJ, Martin S, Nichols RJ. *J Am Chem Soc*, 2010, 132: 2494–2495
83 Leary E, Higgins SJ, van Zalinge H, Haiss W, Nichols RJ, Nygaard S, Jeppesen JO, Ulstrup J. *J Am Chem Soc*, 2008, 130: 12204–12205
84 Liao J, Agustsson JS, Wu S, Schonenberger C, Calame M, Leroux Y, Mayor M, Jeannin O, Ran YF, Liu SX, Decurtins S. *Nano Lett*, 2010, 10: 759–764
85 Baghernejad M, Zhao X, Baruël Ørnsø K, Füeg M, Moreno-García P, Rudnev AV, Kaliginedi V, Vesztergom S, Huang C, Hong W, Broekmann P, Wandlowski T, Thygesen KS, Bryce MR. *J Am Chem Soc*, 2014, 136: 17922–17925
86 Pia EAD, Chi Q, Jones DD, Macdonald JE, Ulstrup J, Elliott M. *Nano Lett*, 2011, 11: 176–182
87 Kay NJ, Higgins SJ, Jeppesen JO, Leary E, Lycoops J, Ulstrup J, Nichols RJ. *J Am Chem Soc*, 2012, 134: 16817–16826
88 Paquette MM, Plaul D, Kurimoto A, Patrick BO, Frank NL. *J Am Chem Soc*, 2018, 140: 14990–15000
89 Li J, Zhao Z, Yu C, Wang H, Zhao J. *J Comput Chem*, 2012, 33: 666–672
90 Darwish N, Díez-Pérez I, Da Silva P, Tao N, Gooding JJ, Paddon-Row MN. *Angew Chem Int Ed*, 2012, 51: 3203–3206
91 Xiang L, Palma JL, Li Y, Mujica V, Ratner MA, Tao N. *Nat Commun*,

2017, 8: 14471
92 Li Y, Wang H, Wang Z, Qiao Y, Ulstrup J, Chen HY, Zhou G, Tao N. *Proc Natl Acad Sci USA*, 2019, 116: 3407–3412
93 Zhang J, Kuznetsov AM, Medvedev IG, Chi Q, Albrecht T, Jensen PS, Ulstrup J. *Chem Rev*, 2008, 108: 2737–2791
94 Capozzi B, Chen Q, Darancet P, Kotiuga M, Buzzeo M, Neaton JB, Nuckolls C, Venkataraman L. *Nano Lett*, 2014, 14: 1400–1404
95 Li Y, Buerkle M, Li G, Rostamian A, Wang H, Wang Z, Bowler DR, Miyazaki T, Xiang L, Asai Y, Zhou G, Tao N. *Nat Mater*, 2019, 18: 357–363
96 Bai J, Daaoub A, Sangtarash S, Li X, Tang Y, Zou Q, Sadeghi H, Liu S, Huang X, Tan Z, Liu J, Yang Y, Shi J, Mészáros G, Chen W, Lambert C, Hong W. *Nat Mater*, 2019, 18: 364–369
97 Huang B, Liu X, Yuan Y, Hong ZW, Zheng JF, Pei LQ, Shao Y, Li JF, Zhou XS, Chen JZ, Jin S, Mao BW. *J Am Chem Soc*, 2018, 140: 17685–17690
98 Zhao Z, Liu R, Mayer D, Coppola M, Sun L, Kim Y, Wang C, Ni L, Chen X, Wang M, Li Z, Lee T, Xiang D. *Small*, 2018, 14: 1703815
99 Zheng J, Liu J, Zhuo Y, Li R, Jin X, Yang Y, Chen ZB, Shi J, Xiao Z, Hong W, Tian ZQ. *Chem Sci*, 2018, 9: 5033–5038